Virus Research 263 (2019) 55–63

Contents lists available at ScienceDirect

Virus Research

journal homepage: www.elsevier.com/locate/virusres

The untranslated regions of EV-A71 contribute to its pathogenicity and virulence

Zhen Dong[a], Zi-Wei Liu[a], Rui Chen[a], Xiao-Jing Wen[a], Jing Ji[a,b], Xue-Xing Zheng[a,b], Li Zhao[a,b], Zhi-Yu Wang[a,b], Hong-Ling Wen[a,b,*]

[a] Department of Microbiological Laboratory Technology, School of Public Health, Shandong University, Jinan, 250012 Shandong Province, China
[b] Key Laboratory for the Prevention and Control of Infectious Diseases (Key Laboratory of China's "13th Five-Year", Shandong University), China

ARTICLE INFO

Keywords:
Enterovirus A71
Untranslated regions
Pathogenicity
Replication capacity

ABSTRACT

Enterovirus A71 (EV-A71) is known for its manifestation as hand foot and mouth disease (HFMD), which has caused countless large-scale epidemic outbreaks throughout the world. However, the molecular pathogenesis of EV-A71 infection is still elusive. Previous studies found that the biological characteristics of a mild EV-A71 strain (SDLY1) and a severe EV-A71 strain (SDLY107) are significantly different, and sequence analysis showed that there are several differences in nucleotide sites of UTRs (88 nt, 123 nt, 143 nt, 154 nt, 187 nt, 241 nt, 243 nt, 253 nt, 291 nt, 438 nt, 440 nt, 571 nt, 579 nt, 602 nt, 658 nt, 664 nt, 690 nt, 696 nt, 7328 nt, 7335 nt, 7367 nt, and 7395 nt). The aim of this study was to determine whether these amino sites in UTRs are associated with the pathogenesis of EV-A71 and are responsible for different clinical manifestations. Based on the reverse genetics technology, we rescued two chimeric viruses SDLY107(1-5'UTR) and SDLY107(1-3'UTR) by replacing 5'UTR/3'UTR gene fragments of an infectious cDNA clone. Replication kinetics and cytotoxicity assays showed that the virulence of the two chimeric strains significantly changed *in vitro*. The viral loads of the two chimeric strains in infected ICR mice were reduced and pathological damage in the brains, lungs, intestinal tissues, and muscles were lightened. Our findings suggest that some nucleotide sites in UTRs may have a function in the pathogenicity and virulence of EV-A71.

1. Introduction

EV-A71 is one of the major causative agents for HFMD, which typically causes vesicles on the palmar and plantar surfaces of the hands and feet, buccal mucosa, tongue, and buttocks. Unlike other pathogens, EV-A71 infections are related to life-threatening neurological diseases such as aseptic meningitis, encephalitis, and poliomyelitis-like paralysis, which can lead to serious complications and put the lives of infected children at risk (Yang et al., 2018; Wang et al., 2018; Liu et al., 2015). Since first being isolated in California in 1969, EV-A71 has caused countless global epidemics. Many large outbreaks especially in the Asia-Pacific regions have recently been described (Liu et al., 2014; Chan et al., 2000; Zander et al., 2014). The molecular pathogenesis of EV-A71 infection is still elusive. Therefore, understanding the specific pathogenesis of EV-A71 is an essential step in the prevention and control of HFMD.

EV-A71 belongs to the *Human Enterovirus A* of the *Picornaviridae* family which contains a huge number of small non-enveloped, positive-sense, single-stranded RNA viruses. The EV-A71 genome is nearly 7400 nucleotides with a long single open reading frame (ORF) in the middle, with 5′ and 3′ untranslated regions on the two sides. A single polyprotein is encoded by the ORF, and viral proteases cleave it into mature viral structural proteins P1 (VP1-VP4) and nonstructural proteins P2 (2 A-2C) and P3 (3A-3D) (Ng et al., 2015; Zhou et al., 2011; Chen et al., 2010). The 5′UTR of the EV-A71 RNA genome is made up of three regions: the 5′ terminal cloverleaf structure, the internal ribosome entry site (IRES) element, and the hypervariable region. The IRES is essential for the translation of the viral mRNA. It has been confirmed that many cellular elemental factors (HnRNP A1, FBP3, and others) can specifically bind to the 5′UTR of EV-A71, thereby significantly regulating viral replication in host cells (Huang et al., 2016; Tolbert et al., 2017). Accumulated reports indicated that the 5′UTR region is one of the virulence determinants, and mutations may affect viral translation and replication, as well as affinity for cellular tissues (Li et al., 2011; Yee et al., 2016; Huang et al., 2014; Malnou et al., 2002). A single nucleotide change of C158U in IRES was proved to attenuate viral

* Corresponding author at: Department of Microbiological Laboratory Technology, School of Public Health, Shandong University, Jinan, 250012 Shandong Province, China.
E-mail address: wenhongling@sdu.edu.cn (H.-L. Wen).

https://doi.org/10.1016/j.virusres.2018.12.019
Received 15 October 2018; Received in revised form 28 December 2018; Accepted 30 December 2018
Available online 03 January 2019
0168-1702/

replication and virulence in mice (Yeh et al., 2011). In addition, several studies indicated that some unique RNA secondary structures are formed in the 5′UTR, and the structural changes and other factors which can affect viral virulence are under investigation (Tolbert et al., 2017; Jia et al., 2016). The 3′UTR region of EV-A71 is also a highly-conserved region and has a variety of complex spatial structures that may contain regulatory sites for the capacity of viral replication. Some research found that partial sequence deletion or internal structural distortion may cause the virus to be temperature sensitive and cause growth defects in cells (Zoll et al., 2009; Ng et al., 2017).

As previously reported, we isolated six EV-A71 strains from HFMD patients and they all clustered into the C4a sub-genotype. One of them was isolated from a fatal neurological case (SDLY107) and one isolated from HFMD patients without neurological complications (SDLY1). They had significant differences in biological characteristics and pathogenicity (Wen et al., 2013; Li et al., 2018a). To identify the determinants of virulence, the regions where the two EV-A71 strains differed were analyzed. The nucleotide sequence comparison between SDLY107 and SDLY1 strains showed 18 different sites in 5′UTR (88 nt, 123 nt, 143 nt, 154 nt, 187 nt, 241 nt, 243 nt, 253 nt, 291 nt, 438 nt, 440 nt, 571 nt, 579 nt, 602 nt, 658 nt, 664 nt, 690 nt, and 696 nt) and 4 different sites in 3′UTR (7328 nt, 7335 nt, 7367 nt, and 7395 nt). We speculated that these sites in UTRs may be associated with the pathogenesis and are responsible for different clinical manifestations. The EV-A71 chimeric strains SDLY107(1-5′UTR) and SDLY107(1-3′UTR) were recombined by replacing 5′UTR/3′UTR gene fragments of the severe strain SDLY107 with those of the mild strain SDLY1 on the basis of an infectious cDNA clone. Then, the replication capacity and cytotoxicity of the two recombinant viruses were studied *in vitro*, and a high temperature group was established to investigate temperature sensitivity. Tissue viral loads and pathological damage were further examined to assess the effect of virulence *in vivo*.

2. Materials and methods

2.1. Cell lines and viruses

RD cells (Rhabdomyosarcoma), SH-SY5Y cells (cloned from SK-N-SH), and U87 cells (Uppsala 87 Malignant Glioma) were selected to comprehensively characterize the effect of UTRs *in vitro*. RD cells are extremely sensitive to EV-A71. U87 cells and SH-SY5Y cells were selected to study the neurotoxicity of EV-A71. RD and SH-SY5Y cells were cultured in Minimum Essential Medium (MEM; Gibco) which was supplemented with 10% heat-inactivated fetal bovine serum (FBS; Gibco), 100U/ml penicillin, and 100 μg/ml streptomycin. Similarly, U87 cells were cultured under the same conditions but in Dulbecco's modified Eagle medium (DMEM; Gibco). All cell lines were cultured in a 37°C incubator with 5% CO_2 until 80%–90% confluency.

As previously reported (Ma et al., 2015), the full-length infectious cDNA clones of SDLY107 strain ($SDLY107^{RV}$) was successfully constructed on the basic of reverse genetics technology. Further studies demonstrated that there was no significant difference in the biological characteristics of wild-type SDLY107 and rescued $SDLY107^{RV}$. Then we performed fragments replacement on the basis of pcDNA3.1(+) SDLY107. The replacement fragments were amplified by overlapping PCR, and ligated into the pcDNA3.1(+) plasmid. The desired fragments were recovered from the recombinant plasmid and pcDNA3.1(+) SDLY107 plasmid after double digestion, and then the recombinant cDNA infectious clone of the recombinant virus was constructed. The recombinant RNA was transfected into RD cells for the preparation of recombinant virus particles.

2.2. Indirect immunofluorescent assay (IFA)

RD cells in a good growth state were seeded in 6-well plates with 70%–80% confluency. They were infected with SDLY1, SDLY107(1-3′UTR), SDLY107(1-5′UTR), and SDLY107 for 24 h. The infected cell monolayers were fixed and incubated with mouse monoclonal antibodies against EV71 (1:200; Abcam, UK) for 1 h. After washing with PBST (PBS-Tween20), the cell monolayers were incubated with goat anti-mouse immunoglobulins conjugated with fluorescein isothiocyanate (1:200, Zsbio, China). The cells were rinsed with PBST and observed under a fluorescence microscope.

2.3. Viral RNA replication curves

RD cells, SH-SY5Y cells, and U87 cells in a good growth state were separately infected with SDLY1, SDLY107(1-3′UTR), SDLY107(1-5′UTR), and SDLY107 at MOI = 0.1PFU/cell. The culture supernatants of RD and U87 cells were sampled every 12 h post infection and SH-SY5Y cells at every 24 h, because SH-SY5Y cells are not as sensitive to EV-A71 as are RD cells. Total viral RNAs were extracted from samples with the E.Z.N.A. Viral RNA Kit (OMEGA, China), according to the manufacturer's recommended protocol. Then, viral RNAs were reverse transcribed into cDNA, and real-time quantitative polymerase chain reactions (RT-qPCR) were carried out using the EV-A71-specific primer pair. The specific method and operation procedure of the RT-qPCR were mentioned in a previous study (Sun et al., 2014). The viral loads were calculated by putting the CT value into a known standard curve, and then line charts were plotted accordingly. All experiments were independently performed at 37°C or 39.5°C in triplicate.

2.4. Cytotoxicity LDH assay

RD cells, SH-SY5Y cells, and U87 cells in a good growth state were seeded in 96-well plates with 70%–80% confluency. They were infected with SDLY1, SDLY107(1-3′UTR), SDLY107(1-5′UTR), and SDLY107 at MOI = 0.1PFU/cell and incubated at 37°C/39.5°C. After 1 h, 1%FBS was added to cell cultures and continuously incubated for 35 h (RD and U87 cells) or 47 h (SH-SY5Y cells). The LDH activity was measured by a Cytotoxicity Assay Kit (Beyotime, China), which evaluated cytotoxicity by detecting the activity of lactate dehydrogenase released into the cultures by the cells. A microplate spectrophotometer was used to measure the absorbance (A) volume of cell supernatants at 490 nm. Each experiment was performed three times with four parallel samples. The results were calculated according to the following equation: (OD_{490} of the treated sample − OD_{490} of the control sample) / (OD_{490} of the maximum LDH activity − OD_{490} of the control sample) × 100.

2.5. Cell proliferation assay

RD cells, SH-SY5Y cells, and U87 cells in a good growth state were cultured in 96-well plates, and infected with the four EV-A71 strains at MOI = 0.1PFU/cell. After 35 h (RD cells and U87 cells) or 47 h (SH-SY5Y cells) incubation, a Cell Counting Kit-8 (Beyotime, China) was used to assay the cell proliferation level. The absorbance (A) volume of cell supernatants at 450 nm was measured using a microplate spectrophotometer. The experiment was performed three times with four parallel samples. The data were calculated based on the following equation: (OD_{450} of the treated sample – OD_{450} of the blank control) / (OD_{450} of the control sample – OD_{450} of the blank control) × 100, as shown in the manufacturer's instruction.

2.6. Virus titer curves

RD cells, SH-SY5Y cells, and U87 cells in a good growth state were infected with the four EV-A71 strains at MOI = 0.1PFU/cell and cultured in a 37°C/39.5°C incubator. 1%FBS was added to the culture supernatants after incubation for 1 h and then culture supernatants were sampled at the indicated time points. The virus titers of cell culture supernatants at each time point were determined by plaque assays. Each experiment was independently performed three times and the data

Table 1
Clinical scoring criteria.

Clinical score	Clinical manifestation
0	Health
1	Fatigue or sleepiness
2	Weight loss and bow back
3	Hind limb weakness or jitter
4	Limb paralysis
5	Dying or death

were expressed as the mean ± SD.

2.7. Animal experiment on ICR mice

All procedures involving animals in this study were in accordance with the guidelines of National Institutes of Health. Our research was reviewed and approved by the Animal Care Use Committee of Shandong University (Approved protocol no.20130305). The ICR mice used in this experiment were obtained from the Pengyue Experimental Animal Breeding Co., Ltd (Jinan, China). In experimental groups, 1-day old ICR mice (n = 14–18) were given an intracerebral injection of SDLY1, SDLY107(1-3′UTR), SDLY(1-5′UTR), or SDLY107 at 1.0×10^4PFU. The negative control group was injected with physiological saline. Cause of death was considered to be nonspecific if it occurred within 24 h of intracerebral injection. The body weights of the mice were determined and clinical symptoms were monitored daily. A line chart of the mean clinical scores was drawn according to the clinical scoring criteria on Table 1.

2.8. The kinetics of replication in ICR mice

The ICR mice were immediately dissected after death to obtain tissue samples in triplicate. Hind limb muscle tissues were collected 1–10 days post infection for monitoring changes of EV-A71 viral loads *in vivo*. The Total RNA Kit II (OMEGA, China) was used to isolate total RNA from the muscle tissues, and all operations were based on the animal tissue protocol in the instructions. The amount of muscle tissues used for total RNA extraction in this experiment was 30 mg. The extracted total RNAs were reverse transcribed into cDNA using the EV-A71-specific primer pair. Quantification was performed by the real-time quantitative polymerase chain reaction.

2.9. Histopathology of EV-A71-infected ICR mice

All experimental mice were immediately dissected after death. Brain, lung, intestine, and muscle tissues were collected daily for histopathological analysis. The collected organs/tissues were placed in a 4% (v/v) paraformaldehyde fixative solution. All fixed tissues/organs were embedded in paraffin blocks and serial 5 mm sections were cut and mounted on glass slides. The pathological sections stained with hematoxylin-eosin (HE) were observed under a biological microscope to evaluate the pathological damage of the tissues.

2.10. Statistical analysis

All experiments were done at least three times, and the data are expressed as means ± SD. All statistical analysis was performed with SPSS 16.0 using the ANOVA test. The P value < 0.01 was considered to indicate statistical significance.

3. Results

3.1. Virus identification

The schematic diagram of the construction of pcDNA3.1(+)SDLY(1-5′UTR) and pcDNA3.1(+)SDLY107(1-3′UTR) is shown in Fig. 1. A typical cytopathic effect was observed after the recombinant RNA was transfected into RD cells. The virus was harvested when the virus titer reached its highest point and then remained steady. After measurement, the virus titers ($CCID_{50}$) of SDLY1, SDLY107(1-3′UTR), SDLY107(1-5′UTR), and SDLY107 were $10^{-6.5}$/ml, $10^{-6.5}$/ml, $10^{-7.7}$/ml, and $10^{-7.7}$/ml, respectively. Then, the two recombinant viruses were identified by sequencing to further confirm that 5′UTR or 3′UTR was successfully replaced by reverse genetics technology with no mutation sites. In addition, indirect immunofluorescent assay results showed that the two recombinant viruses were positive by immunostaining with antibodies against EV71, as shown in Fig. 2. These results showed that the recombinant viruses SDLY107(1-5′UTR) and SDLY107(1-3′UTR) were successfully constructed.

3.2. Viral RNA replication curves of EV-A71 strains

The results of virus RNA replication curves in RD cells, SH-SY5Y cells, and U87 cells are shown in Fig. 3. It can be seen from the results

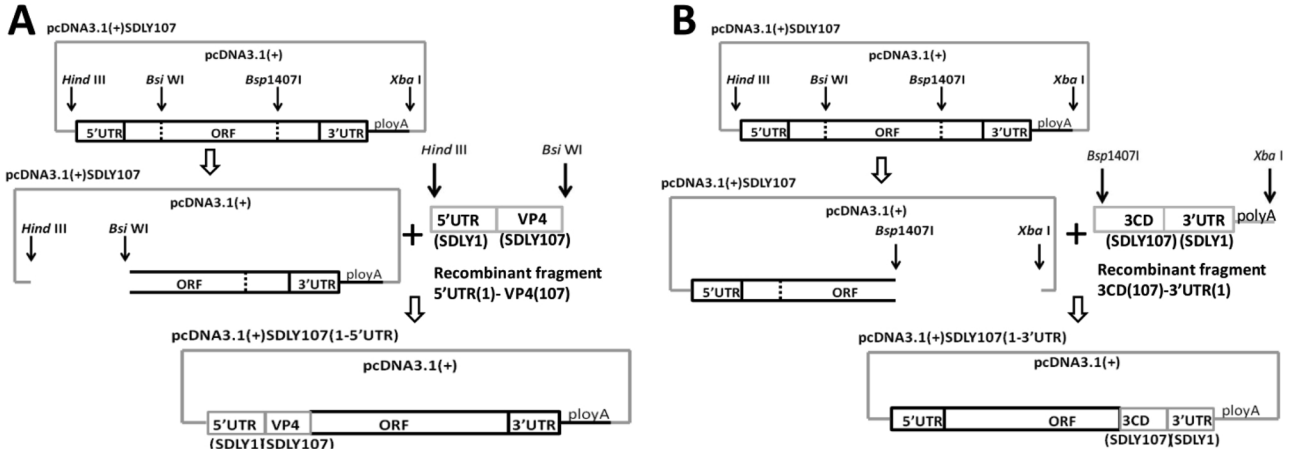

Fig. 1. Schematic diagram of pcDNA3.1(+)SDLY107(1-5′UTR) and pcDNA3.1(+)SDLY107(1-3′UTR). A: The replacement fragment 5′UTR(1)-VP4(107) was amplified by overlapping PCR and ligated into the pcDNA3.1(+) plasmid. The recombinant plasmid and the pcDNA3.1(+)SDLY107 were double digested with *Hind* III and *Bsi* WI, and the target fragment was recovered to construct the recombinant infectious cDNA clone pcDNA3.1(+)SDLY107(1-5′UTR). B: The replacement fragment 3CD(107)-3′UTR(1) was amplified by overlapping PCR and ligated into the pcDNA3.1(+) plasmid. The recombinant plasmid and the pcDNA3.1(+) SDLY107 were double digested with *Bsp*1407I and *Xba* I, and the target fragment was recovered to construct the recombinant infectious cDNA clone pcDNA3.1(+) SDLY107(1-3′UTR).

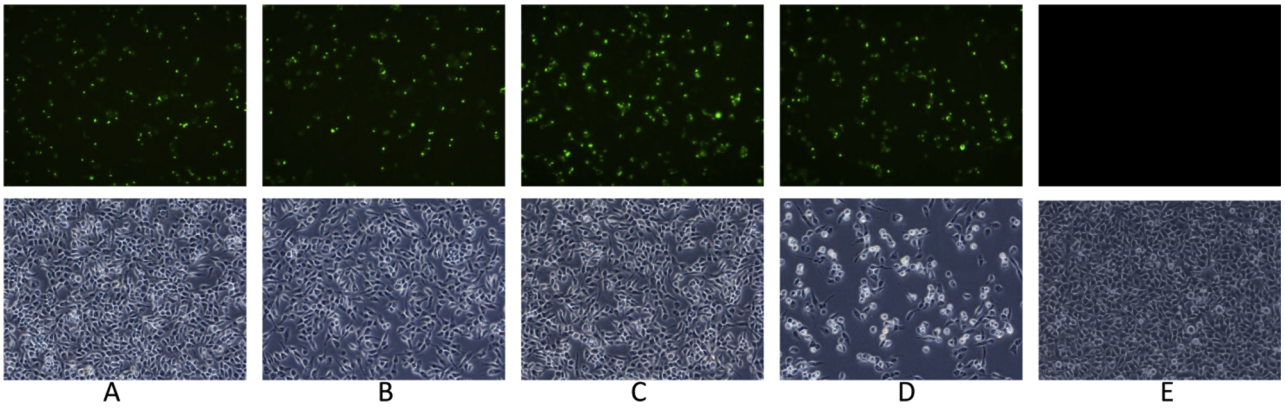

Fig. 2. IFA identification of the recombinant EV-A71 viruses. IFA signals were detected at 24 h in the RD cells infected with the two recombinant viruses, while control cells were negative after treatment with antibodies against EV71. (A, B, C, and D are RD cells infected with SDLY1, SDLY107(1-3′UTR), SDLY107(1-5′UTR), and SDLY107. E is uninfected RD cells.) Images were taken at 200× magnification.

that SDLY107 produced the highest viral loads in the three cell lines both at 37°C and 39.5°C. Also, the viral RNA replication curves of SDLY107(1-5′UTR) and SDLY107(1-3′UTR) were similar to SDLY107 in RD cells and U87 cells. It is worth noting that special results appeared in SH-SY5Y cells. The viral RNA replication curves of SDLY107(1-5′UTR) and SDLY107(1-3′UTR) were obviously lower than both SDLY1 and SDLY107 at 37°C during the observation period though the replication curves eventually rose. We speculated that some nucleotide sites or structures of the replaced UTRs may affect the affinity and infectivity for SH-SY5Y cells, resulting in a lower replication capacity at the beginning. In addition, SDLY107(1-5′UTR) and SDLY107(1-3′UTR) were similar to SDLY1, and lost virus RNA replication capacity in SH-SY5Y cells at 39.5°C. This significant change in replication at high temperature suggested that there were some temperature sensitive sites in the UTRs regions we replaced.

3.3. Cytotoxicity LDH assay

An LDH assay was used to determine the cytotoxicity of the four EV-A71 strains at different temperatures. It can be seen from the results (Fig. 4) that cell injury rates in RD cells at the indicated time points at 37°C were as follows: SDLY107 > SDLY107(1-5′UTR) > SDLY107(1-3′UTR) > SDLY1. Furthermore, the cell injury rates of SDLY107(1-5′UTR) and SDLY107(1-3′UTR) infected groups were significantly weaker than that of SDLY107 and SDLY1 infected groups in U87cells and SH-SY5Y cells at 37°C. In addition, the cell injury results of the three cell lines at 39.5°C were similar to those at 37°C, though cell injury rates were somewhat lower. These findings showed that the cell cytotoxicity of the recombinant virus was attenuated *in vitro*, which was noticeable in the nerve cells. It may imply that some of the previously described differential sites in UTRs are closely linked with the neurotoxicity of EV-A71.

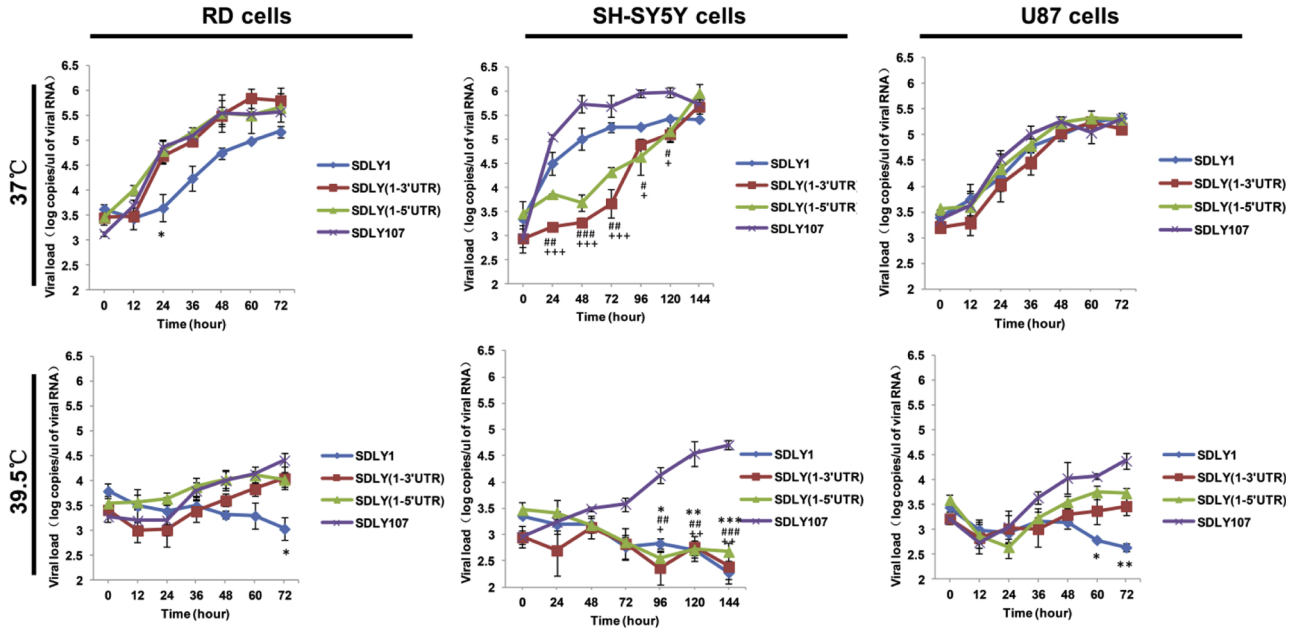

Fig. 3. Viral RNA replication curves of the four EV-A71 strains at 37 °C/39.5 °C. RD, U87, and SH-SY5Y cells were infected with SDLY1, SDLY107(1-3′UTR), SDLY107(1-5′UTR), and SDLY107 at MOI = 0.1PFU/cell. Viral loads in the supernatants of infected cell cultures were detected by RT-qPCR at indicated time points. At each time point, results are expressed as the mean ± SD of three independent experiments with triplicate samples. Statistical analysis was performed using the two-way ANOVA test with the Bonferroni correction. Legends: * statistical analysis between SDLY1 and SDLY107 infected cells; # statistical analysis between SDLY107(1-3′UTR) and SDLY107 infected cells; + statistical analysis between SDLY107(1-5′UTR) and SDLY107 infected cells. * # or + $p < 0.1$, ** ## or ++ $p < 0.01$, *** ### or +++ $p < 0.001$.

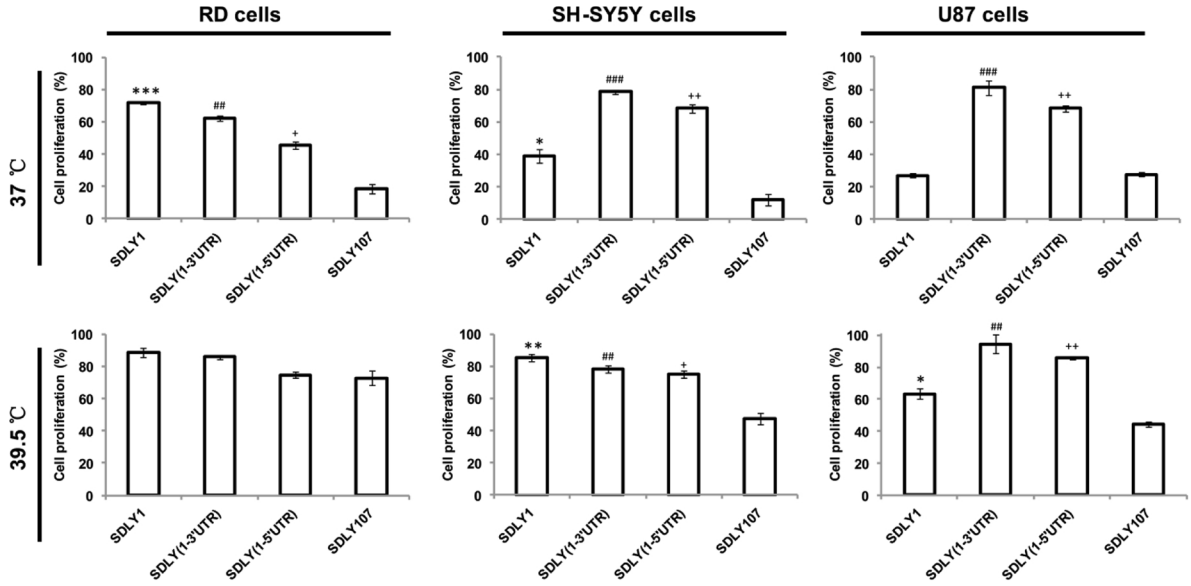

Fig. 4. Cell injury rates of the four EV-A71 strains. RD, U87, and SH-SY5Y cells were infected with SDLY1, SDLY107(1-3′UTR), SDLY107(1-5′UTR), and SDLY107 respectively at MOI = 0.1PFU/cell. The cell injury rate at 37°C/39.5°C was reflected by the lactate dehydrogenase activity of infected cells. Results are expressed as the mean ± SD of four parallel samples. Each experiment was independently repeated three times. Statistical analysis was performed using the one-way ANOVA test. Legends: * statistical analysis between SDLY1 and SDLY107 infected cells; # statistical analysis between SDLY107(1-3′UTR) and SDLY107 infected cells; + statistical analysis between SDLY107(1-5′UTR) and SDLY107 infected cells. * # or + $p < 0.1$, ** ## or ++ $p < 0.01$, *** ### or +++ $p < 0.001$.

3.4. Cell proliferation of EV-A71 strains

The effect of EV-A71 strains on cell proliferation was examined by the CCK-8 assay. According to the results of histograms (Fig. 5), cell proliferation of the four EV-A71 strains in RD cells at 37°C was as follows: SDLY1 > SDLY107(1-3′UTR) > SDLY107(1-5′UTR) > (SDLY107). However, the cell proliferation of SDLY107(1-3′UTR) and SDLY107(1-5′UTR) were higher than those of SDLY1 and SDLY107 in SH-SY5Y and U87 cells, which corresponded to the results of the cell injury rate. At 39.5°C, the cell proliferation rate increased overall, although the cells were not good at high temperatures. These results, together with the results of LDH assays, indicated that the cellular virulence of the recombinant virus had been changed due to the replacement of UTRs. This provided more evidence for the presence of temperature-sensitive and neuron-dependent sites in UTRs.

3.5. Virus titer curves measured by plaque assays

Based on the culture supernatants collected at the indicated time points, we made virus titer curves by plaque assays (Fig. 6). The titer curves of plaque assays were used to indicate the number of infectious virus particles with pathogenic capacity. The severe strain SDLY107 obviously obtained a higher viral titer than the other EV-A71 strains in the three cell lines both at 37°C and 39.5°C. The mild strain SDLY1

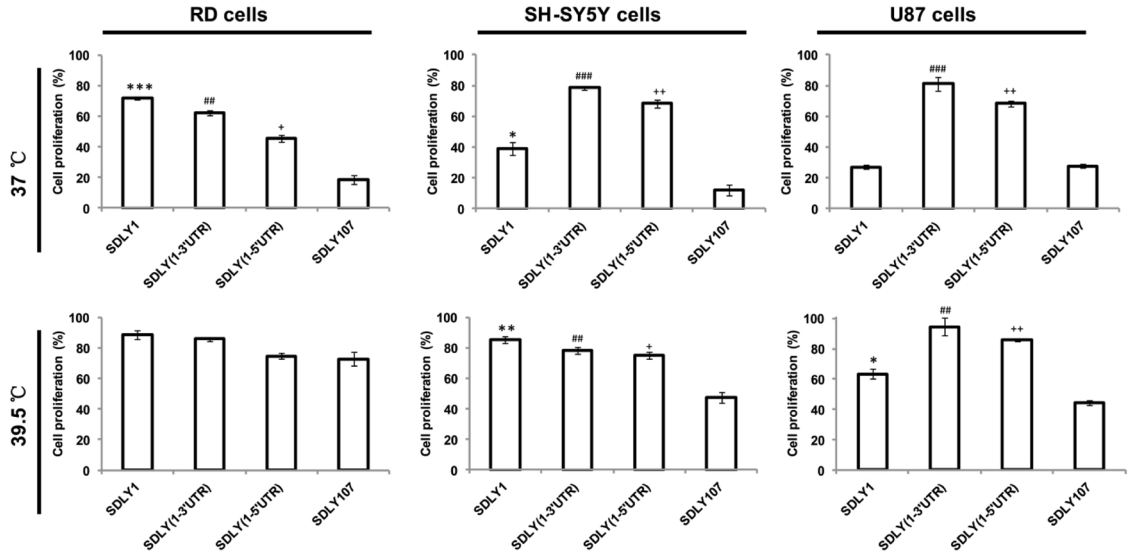

Fig. 5. Cell proliferation rates of the four EV-A71 strains. RD, U87, and SH-SY5Y cells were infected with SDLY1, SDLY107(1-3′UTR), SDLY107(1-5′UTR), and SDLY107 respectively at MOI = 0.1PFU/cell. The cell proliferation rate at 37°C/39.5°C was measured by the Cell Counting Kit-8. Results are expressed as the mean ± SD of four samples. Each experiment was independently repeated three times. Statistical analysis was performed using the one-way ANOVA test. Legends: * statistical analysis between SDLY1 and SDLY107 infected cells; # statistical analysis between SDLY107(1-3′UTR) and SDLY107 infected cells; + statistical analysis between SDLY107(1-5′UTR) and SDLY107 infected cells. * # or + $p < 0.1$, ** ## or ++ $p < 0.01$, *** ### or +++ $p < 0.001$.

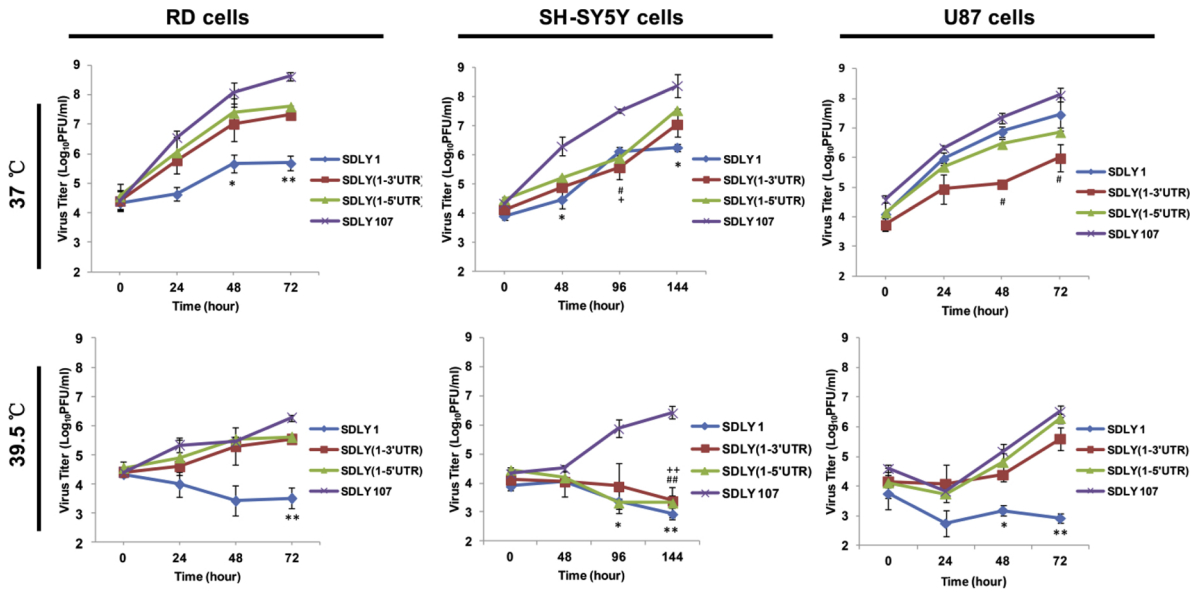

Fig. 6. Viral titers of the four EV-A71 strains. RD, U87, and SH-SY5Y cells were infected with SDLY1, SDLY107(1-3′UTR), SDLY107(1-5′UTR), and SDLY107 at MOI = 0.1PFU/cell. At the indicated time points after infection, virus titers of cell culture supernatants were determined by plaque assays. The results are expressed as the mean ± SD of triplicate samples. Statistical analysis was performed using the two-way ANOVA test. Legends: * statistical analysis between SDLY1 and SDLY107 infected cells; # statistical analysis between SDLY107(1-3′UTR) and SDLY107 infected cells; + statistical analysis between SDLY107(1-5′UTR) and SDLY107 infected cells. * # or + $p < 0.1$, ** ## or ++ $p < 0.01$, *** ### or +++ $p < 0.001$.

generally generated the lowest viral titers in the three cell lines at high temperature. These results correspond to the clinical manifestations of EV-A71 isolated strains, in which patients with neurological complications were more likely to have persistent fever. In addition, the virus titer curves of SDLY107(1-3′UTR) and SDLY107(1-5′UTR) were lower than that of SDLY107 in the three cells, although they replicated equally in U87 and RD cells. This may due to less infectious virus particles or the low cell injury ability of the two chimeric EV-A71 strains in the case of the same replication ability. As expected, only the viral titers curves of SDLY107 rapidly rose in SH-SY5Y cells, but the other three strains did not increase at 39.5°C. In general, the results indicated that some mutation sites in UTRs may affect the pathogenicity or functional affinity to cells, especially in nerve cells.

3.6. The body weight and clinical characteristics of EV-A71-infected mice

During the observation period, the ICR mice infected with the mild strain SDLY1 did not show significant symptoms. But, clinical signs of the ICR mice infected with the severe strain SDLY107 were quickly exhibited, including extreme lethargy, poor activity, hind limb paralysis, but no death. This proved that SDLY107 which was isolated from a fatal case is pathogenic to ICR mice. Typical hind limb paralysis symptom and body weight loss can be seen in the Fig. 7. All symptoms in the ICR mice began to improve at 4 days post infection and eventually disappeared. The ICR mice infected with the two recombinant viruses only exhibited mild symptoms, and the symptoms appeared later. The figure of mean clinical scores of EV-A71-infected ICR mice was drawn according to the clinical scoring criteria (Fig. 7B). In addition, body weight changes of the ICR mice are shown in the Fig. 7C. The data showed that the body weights and growth of the mice infected with the two recombinant viruses were significantly slower than those of the SDLY107 infected group, indicating that some previously described differential sites in UTRs can affect the pathogenicity and performance of clinical characteristics of EV-A71.

3.7. Replication kinetics of EV-A71-infected ICR mice

Specific DNA fragments (226bp) of EV-A71 were detected by RT-PCR in the isolation of total RNA from brain, lung, intestine, and muscle tissues (Fig. 8A). Clinical characteristics in our study showed that EV-A71 strains had strong cytotoxicity in the muscles, so we decided to detect the changes of viral loads in the hind limb muscles by RT-qPCR (Fig. 8B). On the whole, the four EV-A71 strains rapidly replicated in the muscles and the overall trends of replication kinetic curves were similar. Among them, the severe strain SDLY107 had the strongest replication capacity which was reflected both in the replication speed and viral load (5.8×10^3 copies/mg at 3 days post infection). However, replication kinetic curves of the two recombinant viruses increased more slowly and the peak was lower than that of SDLY107. These results further demonstrated that some nucleotide sites in UTRs modulate the replication capacity *in vivo*.

3.8. Histopathology of EV-A71-infected ICR mice

The HE-stained pathological sections were observed under microscope to evaluate the pathological damage of the tissues. Brain, lung, intestine, and muscle tissues of the ICR mice all showed obvious lesions after EV-A71 infection (Fig. 9). Sections taken from corresponding sites in the negative control group appeared normal. It can be seen from the brain sections that there were eosinophil accumulation, neuronal necrosis, and a softening phenomenon (Fig. 9[A–E]). The pathological damage in the brain of SDLY107-infected mice was the most serious, which manifested as diffuse bleeding and a neuronophagia phenomenon. Moreover, alveolar wall interstitial thickening, pulmonary capillaries, and alveolar hemorrhage or alveolar structure destruction of the lung tissue can be observed (Fig. 9[F–J]). Also, the small intestinal mucosal structure was obviously destroyed, which mainly manifested as vacuolar changes in epithelial cells and sparse or shedding of the intestinal villi (Fig. 9[K–O]). Furthermore, the pathological changes of muscle tissues were mainly shown as tissue edema, bleeding and inflammatory cell infiltration progression, muscle fiber disorder, or partial dissolution (Fig. 9[P–T]). In conclusion, the pathological damage of the two recombinant virus groups was slightly milder than the SDLY107 infected group and more severe than the SDLY1 infected group. However, we believe that there might be other virulence determinants in EV-A71.

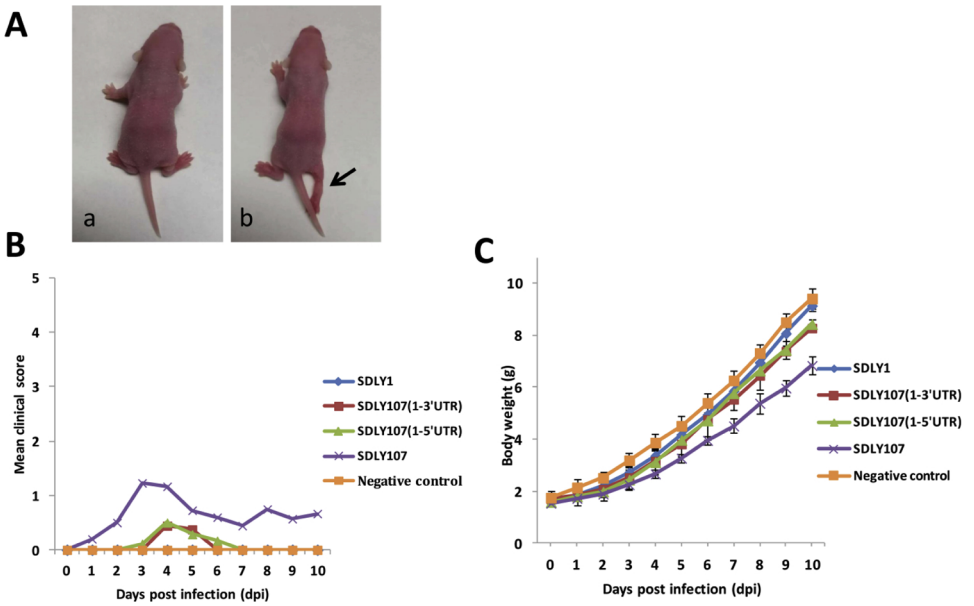

Fig. 7. Clinical symptoms, mean clinical scores, and body weights of EV-A71-infected ICR mice. One-day old ICR mice were infected with physiological saline, 1.0×10^4PFU of SDLY1, 1.0×10^4PFU of SDLY107(1-3′UTR), 1.0×10^4PFU of SDLY107(1-5′UTR), or 1.0×10^4PFU of SDLY107, and mice were monitored daily for clinical symptoms and weight changes. A: ICR mice of the negative control group (a) and EV-A71-infected mice (b) which developed hind-limb paralysis at 2 dpi. The black arrow indicates the paralyzed hind limb. B: Mean clinical scores (n = 3–7 mice). Clinical scores were defined as follows: 0, healthy; 1, fatigue or sleepiness; 2, weight loss and bow back; 3, hind limb weakness or jitter; 4, limb paralysis; 5, dying or death. C: Body weight changes of EV-A71-infected ICR mice (n = 3–7). The data are expressed as the mean ± SD.

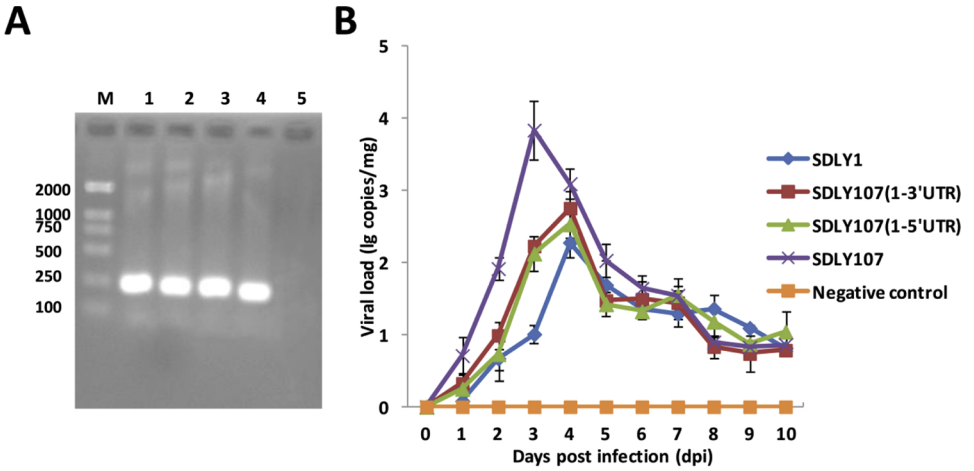

Fig. 8. Detection and quantification of EV-A71 strains in ICR mice. Brain, lung, intestine, and muscle tissues of EV-A71 infected mice were collected daily in triplicate. The total cellular RNA was extracted from tissues and then analyzed by RT-PCR using primers specific for EV-A71. A: RT-PCR results of SDLY107 infected tissues. The results of SDLY1, SDLY107(1-3′UTR), and SDLY107(1-5′UTR) are not shown. (M: DL2000 Marker; Line 1-4: brain, lung, intestine, and muscle tissues. Line 5: negative control.) B: Replication kinetics of muscle tissue in EV-A71-infected mice. The data are expressed as the mean ± SD of three samples. Errors bars represent the SD from triplicate within one experiment.

4. Discussion

EV-A71 is a pathogen of HFMD, which typically causes concentrated infections in children of five years of age or younger. The EV-A71 isolates may lead to diverse clinical outcomes, but the determinants of EV-A71 virulence are unclear. Studies showed that the UTRs of EV-A71 can interact with the cellular RNA binding proteins and have a special regulatory role in viral infection during the initial phase of viral RNA synthesis and protein translation (Tolbert et al., 2017; Zoll et al., 2009), but specific regions or nucleotide sites have not been identified. The predicted secondary structure of 5′UTR showed that the mutation of 488 nt was associated with virulence by influencing the stability of the IRES (Li et al., 2011). In the present study, we confirmed the hypotheses that certain sites in UTRs of EV-A71 contribute to its pathogenicity and virulence. Our work showed that the replication capacity and cell/tissue damage of the two recombinant viruses were changed due to the replacement of 5′UTR/3′UTR, both *in vitro* and *in vivo*. It is undeniable that UTRs of EV-A71 are one of the determinants of virulence. This provides the basis for further confirmation of specific virulence sites in UTRs.

Similar to other neurotropic viruses, EV-A71 strains exhibit neurotropism and are responsible for severe neurological complications, but the precise mechanism remains obscure. Neuronal damage induced by viral infection was shown to be associated with clinical manifestation and disease progression (Markus et al., 2015; Myint et al., 2014). To characterize the neurological effects of UTRs *in vitro,* U87cells and SH-SY5Y cells were selected in this study. It can be seen from our results that cytotoxicity to nerve cells was more serious than to RD cells, especially at high temperatures. Different results observed in the three cell lines indicated that EV71 infection is neuron-dependent. Similarly, it was found that EV-A71 infection preferentially caused cell death in neurons but its clinical importance and implication is unclear (Chang et al., 2015). Some studies provided a new idea for further study of neuron-dependence, in that autophagy was markedly up-regulated in motor neuron-like cells (Too et al., 2016). Amino acid variation of EV-A71 VP1-145 was found to affect the neurovirulence in transgenic mice by altering the viral binding to heparan sulfate (HS) (Kobayashi et al., 2018). Obviously, it is essential to identify the neurovirulent sites of EV-A71 and clarify their mechanisms.

In this study, we rescued two recombinant viruses and analyzed the effect of UTRs on viral RNA replication and cytotoxicity. Our data demonstrated that the replication capacity of the two recombinant viruses was significantly reduced in SH-SY5Y cells. We speculated that some sites or structures of the replaced 5′UTR/3′UTR may affect the affinity and infectivity for SH-SY5Y cells, resulting in a decrease in replication capacity. Moreover, both CCK-8 and LDH assays showed that the cytotoxicity effect of the two recombinant viruses on the three cells was significantly weakened. Together, these results indicated that the

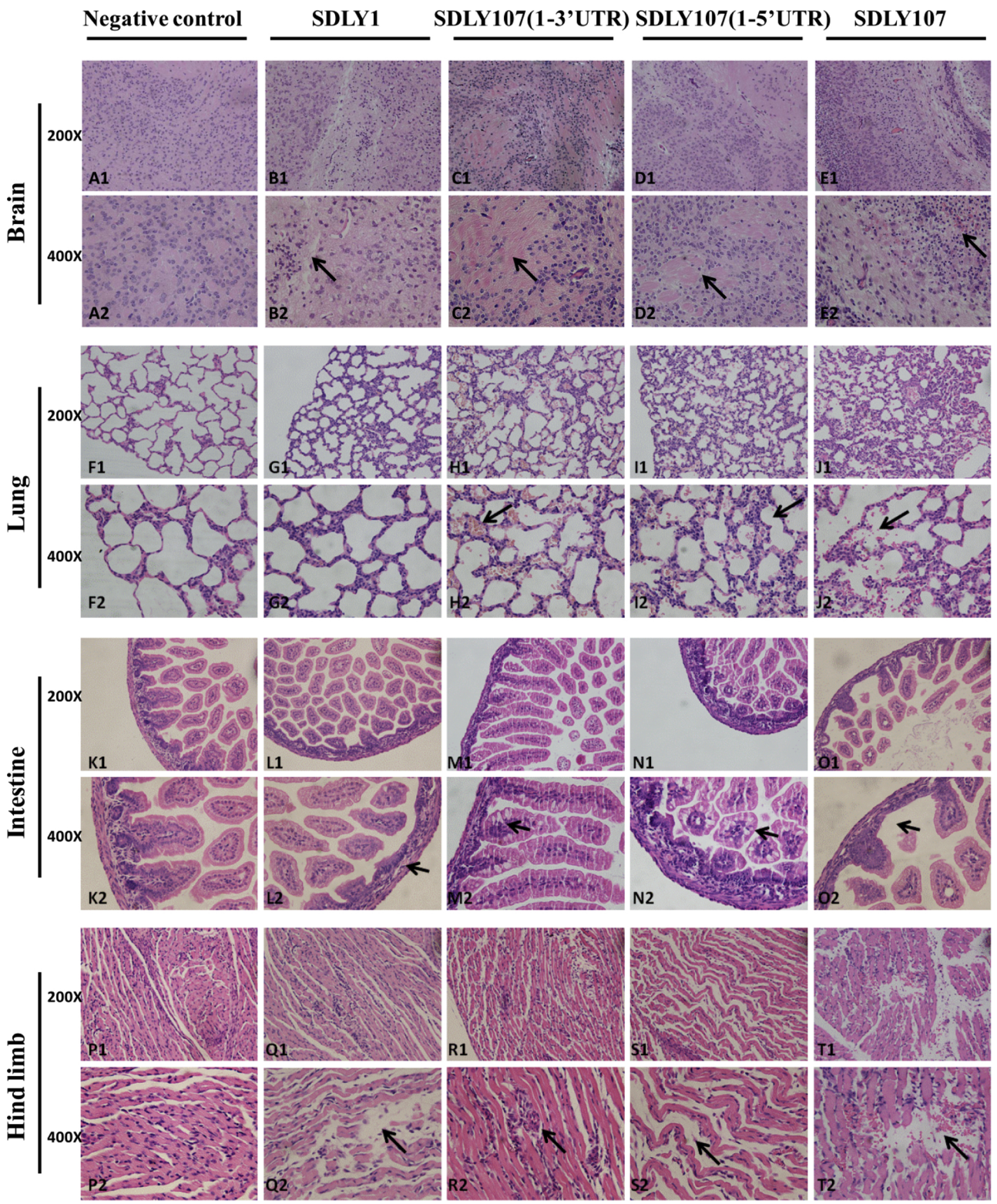

Fig. 9. Histopathology analysis of EV-A71-infected ICR mice. Brain, lung, intestine, and muscle tissues of EV-A71 infected mice were collected daily. Paraffin section of tissues at the indicated time points post-infection were stained with hematoxylin-eosin (HE) and observed under a light microscope. All observations were made at 200× magnification. Representative views are shown at 400× magnification and black arrows indicate the typical lesion. Pathological damages were observed in the four tissues of ICR mice infected with the four EV-71 strains. In general, mice infected with the two recombinant virus exhibited lighter pathological damage than those infected with SDLY107.

virulence of the recombinant viruses was changed due to the replacement of UTRs. This might be a result of the action or co-action of some previously described differential sites in UTRs. In addition, the cell injury was obvious in nerve cells at 39.5°C, suggesting that the neurotoxicity of EV-A71 cannot be ignored in clinical treatment during high fever.

Furthermore, the animal experiments proved our hypothesis that UTRs play a role in EV-A71 pathogenicity. The pathological lesions

induced by the severe and the mild strain were different, indicating that EV-A71 strains have different susceptibility to the organism due to the strong immune system in ICR mice. This showed that the viral replication capabilities of the two recombinant viruses were decreased and clinical symptoms were not as significant as the severe strain SDLY107. The histopathological damage observed in different tissues of mice caused by the two recombinant viruses was slightly milder than that of SDLY107, suggesting that the replacement of UTRs affects the virulence to some extent *in vivo*. It is undeniable that there might be other virulence determinants in EV-A71. Moreover, the ICR mice infected with EV-A71 strains exhibited poor activity and paralysis but not death. These diverse symptoms in the ICR mice and in human patients indicate the complexity of the pathogenesis of EV-A71. An appropriate animal model for understanding clinical prognosis of the severe and mild EV-A71 infection is under exploration. Neonatal mice and monkey animal models of EV-A71 infection were explored in previous studies (Yu et al., 2017; Lin et al., 2013). In addition, an oral Mongolian gerbil model for EV-A71 strains was established, which may be a suitable new model to explore clues of EV-A71 distribution and pathogenesis (Li et al., 2018b).

In summary, we demonstrated that UTRs of EV-A71 contribute its pathogenicity and virulence. This may be partly responsible for the replication capacity (*in vitro* and *in vivo*) or neurovirulence of EV-A71. Analysis of differential sites in UTRs (88 nt, 123 nt, 143 nt, 154 nt, 187 nt, 241 nt, 243 nt, 253 nt, 291 nt, 438 nt, 440 nt, 571 nt, 579 nt, 602 nt, 658 nt, 664 nt, 690 nt, 696 nt, 7328 nt, 7335 nt, 7367 nt, and 7395 nt) of SDLY107 and SDLY1 may find virulent determinants in the future. Our results provide a basis for further confirmation of specific virulence sites in UTRs. Also, we will further study the mode of action of UTRs in EV-A71 and EV-A71-related HFMD concerning the specific molecular mechanism.

Conflicts of interest

The authors declare no financial conflicts of interest.

Acknowledgments

We thank Dr. Edward C. Mignot, Shandong University, for linguistic advice. The work reported here was supported by the National Natural Science Foundation of China (81371833) and Natural Science Foundation of Shandong Province (ZR2018MH035; “Molecular mechanism of enterovirus 71 induced-autophagy”).

References

Chan, L.G., Parashar, U.D., Lye, M.S., Ong, F.G., Zaki, S.R., Alexander, J.P., Ho, K.K., Han, L.L., Pallansch, M.A., Suleiman, A.B., Jegathesan, M., Anderson, L.J., 2000. Deaths of children during an outbreak of hand, foot, and mouth disease in sarawak, malaysia: clinical and pathological characteristics of the disease. For the Outbreak Study Group. Clin. Infect. Dis. 31 (3), 678–683.

Chang, C.Y., Li, J.R., Ou, Y.C., Chen, W.Y., Liao, S.L., Raung, S.L., Hsiao, A.L., Chen, C.J., 2015. Enterovirus 71 infection caused neuronal cell death and cytokine expression in cultured rat neural cells. IUBMB Life 67 (10), 789–800.

Chen, X., Zhang, Q., Li, J., Cao, W., Zhang, J.X., Zhang, L., Zhang, W., Shao, Z.J., Yan, Y., 2010. Analysis of recombination and natural selection in human enterovirus 71. Virology 398 (2), 251–261.

Huang, S.W., Cheng, H.L., Hsieh, H.Y., Chang, C.L., Tsai, H.P., Kuo, P.H., Wang, S.M., Liu, C.C., Su, I.J., Wang, J.R., 2014. Mutations in the non-structural protein region contribute to intra-genotypic evolution of enterovirus 71. J. Biomed. Sci. 21, 33.

Huang, H.I., Chang, Y.Y., Lin, J.Y., Kuo, R.L., Liu, H.P., Shih, S.R., Wu, C.C., 2016. Interactome analysis of the EV71 5’ untranslated region in differentiated neuronal cells SH-SY5Y and regulatory role of FBP3 in viral replication. Proteomics 16 (17), 2351–2362.

Jia, Q.J., Chen, X.Y., Li, Z., Xu, J.J., Xu, Z.G., Duan, Z.L., Wen, J.S., 2016. Comparative genomic analysis of enterovirus 71 revealed six new potential neurovirulence-associated sites. Biomed. Environ. Sci. 29 (10), 767–772.

Kobayashi, K., Sudaka, Y., Takashino, A., Imura, A., Fujii, K., Koike, S., 2018. Amino acid variation at VP1-145 of enterovirus 71 determines attachment receptor usage and neurovirulence in human scavenger receptor B2 transgenic mice. J. Virol.

Li, R., Zou, Q., Chen, L., Zhang, H., Wang, Y., 2011. Molecular analysis of virulent determinants of enterovirus 71. PLoS One 6 (10), e26237.

Li, C., Qiao, Q., Hao, S.B., Dong, Z., Zhao, L., Ji, J., Wang, Z.Y., Wen, H.L., 2018a. Nonstructural protein 2A modulates replication and virulence of enterovirus 71. Virus Res. 244, 262–269.

Li, C.X., Zhang, B., Feng, Y., Xu, C.P., Jiang, J.M., Lu, Y.Y., 2018b. Establishment and characterization of an oral gerbil model for a non-mouse-adapted enterovirus 71 strain. Virus Res. 255, 117–126.

Lin, Y.W., Yu, S.L., Shao, H.Y., Lin, H.Y., Liu, C.C., Hsiao, K.N., Chitra, E., Tsou, Y.L., Chang, H.W., Sia, C., Chong, P., Chow, Y.H., 2013. Human SCARB2 transgenic mice as an infectious animal model for enterovirus 71. PLoS One 8 (2), e57591.

Liu, N., Xie, J., Qiu, X., Jia, L., Wu, Z., Ma, Y., Wang, Z., Li, P., Ren, X., Hao, R., Wang, L., Wang, Y., Qiu, S., Song, H., 2014. An atypical winter outbreak of hand, foot, and mouth disease associated with human enterovirus 71, 2010. BMC Infect. Dis. 14, 123.

Liu, B., Luo, L., Yan, S., Wen, T., Bai, W., Li, H., Zhang, G., Lu, X., Liu, Y., He, L., 2015. Clinical features for mild hand, foot and mouth disease in China. PLoS One 10 (8), e0135503.

Ma, Y.W., Hao, S.B., Sun, L.L., Li, J., Qiao, Q., Gao, F., Zhao, L., Yu, X.J., Wang, Z.Y., Wen, H.L., 2015. Construction and characterization of infectious cDNA clones of enterovirus 71 (EV71). Virol. Sin. 30 (4), 305–308.

Malnou, C.E., Poyry, T.A., Jackson, R.J., Kean, K.M., 2002. Poliovirus internal ribosome entry segment structure alterations that specifically affect function in neuronal cells: molecular genetic analysis. J. Virol. 76 (21), 10617–10626.

Markus, A., Lebenthal-Loinger, I., Yang, I.H., Kinchington, P.R., Goldstein, R.S., 2015. An in vitro model of latency and reactivation of varicella zoster virus in human stem cell-derived neurons. PLoS Pathog. 11, e10048856.

Myint, K.S.A., Kipar, A., Jarman, R.G., Gibbons, R.V., Perng, G.C., Flanagan, B., Mongkolsirichaikul, D., Van Gessel, Y., Solomon, T., 2014. Neuropathogenesis of Japanese Encephalitis in a primate model. PLoS Neql. Trop. Dis. 8, e29808.

Ng, Q., He, F., Kwang, J., 2015. Recent progress towards novel EV71 anti-therapeutics and vaccines. Viruses 7 (12), 6441–6457.

Ng, W.C., Soto-Acosta, R., Bradrick, S.S., Garcia-Blanco, M.A., Ooi, E.E., 2017. The 5’ and 3’ untranslated regions of the flaviviral genome. Viruses 9 (6).

Sun, L.L., Wang, J.K., Cui, X.Q., Hao, S.B., Li, J., Zhao, L., Yuan, X.J., Wen, H.L., Yu, X.J., Wang, Z.Y., 2014. Association of viral replication capacity with the pathogenicity of enterovirus 71. Virus Res. 189, 1–7.

Tolbert, M., Morgan, C.E., Pollum, M., Crespo-Hernandez, C.E., Li, M.L., Brewer, G., Tolbert, B.S., 2017. HnRNP A1 alters the structure of a conserved enterovirus IRES domain to stimulate viral translation. J. Mol. Biol. 429 (19), 2841–2858.

Too, I.H.K., Yeo, H., Sessions, O.M., Yan, B., Libau, E.A., Howe, J.L.C., Lim, Z.Q., Sukumaran, S., Ong, W., Chua, K.B., Wong, B.S., Chow, V.T.K., Alonso, S., 2016. Enterovirus 71 infection of motor neuron-like NSC-34 cells undergoes a non-lytic exit pathway. Sci. Rep. 6 (36983).

Wang, J., Teng, Z., Cui, X., Li, C., Pan, H., Zheng, Y., Mao, S., Yang, Y., Wu, L., Guo, X., Zhang, X., Zhu, Y., 2018. Epidemiological and serological surveillance of hand-foot-and-mouth disease in Shanghai, China, 2012–2016. Emerg. Microbes Infect. 7 (1), 8.

Wen, H.L., Si, L.Y., Yuan, X.J., Hao, S.B., Gao, F., Chu, F.L., Sun, C.X., Wang, Z.Y., 2013. Complete genome sequencing and analysis of six enterovirus 71 strains with different clinical phenotypes. Virol. J. 10, 115.

Yang, S.D., Li, P.Q., Huang, Y.G., Li, W., Ma, L.Z., Wu, L., Wang, N., Lu, J.M., Chen, W.Q., Liu, G.M., Xiong, Y.M., Chen, Y.L., Zhang, Y., 2018. Factors associated with fatal outcome of children with enterovirus A71 infection: a case series. Epidemiol. Infect. 146 (6), 788–798.

Yee, P.T., Tan, K.O., Othman, I., Poh, C.L., 2016. Identification of molecular determinants of cell culture growth characteristics of Enterovirus 71. Virol. J. 13 (1), 194.

Yeh, M.T., Wang, S.W., Yu, C.K., Lin, K.H., Lei, H.Y., Su, I.J., Wang, J.R., 2011. A single nucleotide in stem loop II of 5’-untranslated region contributes to virulence of enterovirus 71 in mice. PLoS One 6 (11), e27082.

Yu, P., Bao, L., Xu, L., Li, F., Lv, Q., Deng, W., Xu, Y., Qin, C., 2017. Neurotropism in vitro and mouse models of severe and mild infection with clinical strains of enterovirus 71. Viruses 9 (11).

Zander, A., Britton, P.N., Navin, T., Horsley, E., Tobin, S., McAnulty, J.M., 2014. An outbreak of enterovirus 71 in metropolitan Sydney: enhanced surveillance and lessons learnt. Med. J. Aust. 201 (11), 663–666.

Zhou, F., Kong, F., Wang, B., McPhie, K., Gilbert, G.L., Dwyer, D.E., 2011. Molecular characterization of enterovirus 71 and coxsackievirus A16 using the 5’ untranslated region and VP1 region. J. Med. Microbiol. 60 (Pt. 3), 349–358.

Zoll, J., Heus, H.A., van Kuppeveld, F.J., Melchers, W.J., 2009. The structure-function relationship of the enterovirus 3’-UTR. Virus Res. 139 (2), 209–216.